Journal of Advanced Ceramics
2017, **6**(1): 20–26
DOI: 10.1007/s40145-016-0212-2

ISSN 2226-4108
CN 10-1154/TQ

Research Article

Understanding microwave dielectric properties of $(1-x)CaTiO_3$–$xLaAlO_3$ ceramics in terms of A/B-site ionic-parameters

Zhanming DOU†, Gan WANG†, Juan JIANG*, Fan ZHANG, Tianjin ZHANG*

Hubei Collaborative Innovation Center for Advanced Organic Chemical Materials, *Ministry of Education Key Laboratory for the Green Preparation and Application of Functional Materials and School of Material Science and Engineering*, *Hubei University*, *Wuhan 430062*, *China*

Received: April 09, 2016; Revised: October 21, 2016; Accepted: October 23, 2016

Abstract: We prepared $(1-x)CaTiO_3$–$xLaAlO_3$ ($0 \leqslant x \leqslant 1$) microwave dielectric ceramics using a conventional two-step solid-state reaction method, and investigated microwave dielectric properties of the ceramics in terms of A/B-site ionic-parameters. Ionic-parameters such as ionic polarizability, A-site bond valence, and ionic rattling were linked to the microwave dielectric properties. As the $LaAlO_3$ content x in the $(1-x)CaTiO_3$–$xLaAlO_3$ ceramics increased from 0.3 to 0.7, the dielectric constant gradually decreased, which was attributed to the decrease of polarizability deviation and suppression of the cation rattling. The temperature coefficient of the resonant frequency decreased as the content of $LaAlO_3$ increased because of the increase of A-site cation bond valence. The quality factor value ($Q \times f$) increased as $LaAlO_3$ content increased because of the enhancement of the order degree of B-site cation. A significant deterioration of the temperature coefficient of the resonant frequency and $Q \times f$ value was observed at the composition $x = 0.5$. These decreases were attributed to a phase transition from orthorhombic crystal (for $x \leqslant 0.5$) to rhombohedral crystal (for $x > 0.5$).

Keywords: $(1-x)CaTiO_3$–$xLaAlO_3$ (CTLA) microwave dielectric ceramics; ionic polarizability; bond valence; cation rattling effect

1 Introduction

Modern wireless communication devices, such as filters, oscillators, and dielectric resonators, require microwave dielectric ceramics with appropriate dielectric constant ($\varepsilon_r \approx 45$), high quality factor value ($Q \times f > 30\,000$ GHz), and near-zero temperature coefficient of resonant frequency ($\tau_f \approx 0$) [1–3]. To meet the requirements of current and future systems, the perovskite family of materials have been extensively studied among a number of dielectric material systems. τ_f-compensated $CaTiO_3$–$REAlO_3$ ceramics (where RE denotes a rare earth element) have attracted attention as a typical microwave dielectric ceramic family with perovskite structure, because most rare earth aluminates have suitable dielectric constant and high quality factor value but large negative temperature coefficient, while $CaTiO_3$ ceramics are characterized with $\varepsilon_r \approx 160$, $Q \times f \approx 7000$ GHz, and $\tau_f \approx +850$ ppm/℃ [4]. However, large-scale production of these materials has been limited because preparation of most $CaTiO_3$–$REAlO_3$

† These authors contributed equally to this work.
* Corresponding authors.
E-mail: T. Zhang, zhangtj@hubu.edu.cn;
J. Jiang, jiangjuan@hubu.edu.cn

ceramics requires high sintering temperature (>1450℃) and because of the high cost of rare earth elements [5]. Among $CaTiO_3$–$REAlO_3$ materials, $CaTiO_3$–$LaAlO_3$ stands out as a candidate with suitable microwave dielectric properties that could meet the need of microwave dielectric filters used in mobile communication base stations because of the good thermal stability of the ceramics [6,7] and the relatively low cost of the starting materials.

Moon *et al*. [8] and Hou *et al*. [9] investigated the sintering behaviour and microwave dielectric properties of xCaTiO$_3$–(1−x)LaAlO$_3$ ceramics, and Khalyavin *et al*. [10] studied the structure sequence transformation of xCaTiO$_3$–(1−x)LaAlO$_3$ ceramics. These studies focused on the direct relation between composition and microwave dielectric properties in this system. The origin of ε_r, $Q\times f$, and τ_f in xCaTiO$_3$–(1−x)LaAlO$_3$ ceramics, i.e., ionic-parameters such as ionic polarizability, A-site bond valence, and cation rattling, have not been widely reported. In other ceramic families, ionic-parameters have been linked to the microwave dielectric properties. For example, Zhang *et al*. [11] suggested that the dielectric constant of $(Mg_{1-x}Ni_x)_2SiO_4$ decreases as x increases because the ionic polarizablility of Ni^{2+} (1.23 Å^3) is less than that of Mg^{2+} (1.32 Å^3). The effect of the bond valence on τ_f has also been studied. The effect of A-site bond valance on the variation of τ_f value of $(Zn_{1-x}Ni_x)_3Nb_2O_8$ ceramics has been discussed by Huang *et al*. [12]. Li *et al*. [13] discovered that τ_f decreases as the difference between the A- and B-site bond valences increases, i.e., as the $(Li_{0.5}La_{0.5})TiO_3$ content increases. To understand the effect of composition on the microwave dielectric properties of (1−x)CaTiO$_3$–xLaAlO$_3$ ceramics and to tailor their microwave dielectric properties, the correlation between the microwave dielectric properties and ionic-parameters such as polarizability, cation rattling effect, bond valence, and the order degree of B-site cation must be understood.

In this work, (1−x)CaTiO$_3$–xLaAlO$_3$ (CTLA, $0\leqslant x\leqslant 1$) ceramics were prepared using a conventional two-step solid-state reaction method. The relationship between the microwave dielectric properties and ionic-parameters was established, and the microwave dielectric properties of CTLA ceramics with $0.3\leqslant x\leqslant 0.7$ were discussed.

2 Experimental

2.1 Sample preparation

CTLA ceramics were prepared using a conventional two-step solid-state reaction method from high-purity $CaCO_3$ (99.3%), TiO_2 (99.9%), La_2O_3 (99.99%), and Al_2O_3 (94%). $CaTiO_3$ was calcined at 1090 ℃ for 6 h and $LaAlO_3$ was calcined at 1200 ℃ for 5 h. The fully-stoichiometric calcined powders were weighed and ground using ball milling for 8 h, dried at 120 ℃ for 12 h, and then mixed with 5 wt% polyvinyl alcohol (PVA) solution as a binder. The final powders were uniaxially pressed into Φ12 mm × 6 mm cylinders. The samples were heated at 650 ℃ to remove the PVA binder and then sintered at 1450 ℃ for 4 h in air. The furnace was cooled from the sintering temperature to 1000 ℃ at 2 ℃/min and then the ceramics were allowed to cool naturally.

2.2 Characterization and theoretical analysis

The crystal structure of the sintered samples was characterized via X-ray powder diffraction (XRD) using a Bruker advanced X-ray powder diffractometer and Cu Kα radiation. Lattice parameters were determined from Rietveld structure refinement of the XRD data using the TOPAS software. The apparent densities of the ceramics were measured using the Archimedes method. The microstructures of the ceramics were examined using a JEOL JSM-7100F scanning electron microscope (SEM). The Raman spectra were collected using a Horiba Jobin Yvon HR800 with a laser wavelength of 488 nm, and the Si peak at 520 cm^{-1} was used for pre-calibration. The microwave dielectric properties of the ceramics were measured with an Agilent E5071C network analyzer using the cavity reflection method. τ_f was calculated between −20 and 65 ℃ as

$$\tau_f=\frac{f_{(T_2)}-f_{(T_1)}}{f_{(T_1)}(T_2-T_1)} \tag{1}$$

where $f_{(T_1)}$ is the resonant frequency at −20 ℃ and $f_{(T_2)}$ is the resonant frequency at 65 ℃. Deviations of polarizability (Δ%) were calculated as

$$\Delta\%=\frac{\alpha_{\text{obs.}}-\alpha_{\text{theo.}}}{\alpha_{\text{theo.}}}\times 100 \tag{2}$$

where $\alpha_{\text{theo.}}$ was calculated using the additivity rule of dielectric polarizabilities as [4]:

$$\alpha_{\text{theo.}}(ABO_3) = \alpha_A + \alpha_B + 3\alpha_O \quad (3)$$

where α_A, α_B, and α_O are the ionic polarizabilities of A-site ion, B-site ion, and oxygen, respectively. $\alpha_{\text{obs.}}$ was obtained using the Clausius–Mossotti equation [14]:

$$\alpha_{\text{obs.}} = \frac{V_m(\varepsilon_r - 1)}{b(\varepsilon_r + 2)} \quad (4)$$

where ε_r is the measured dielectric constant, b is 4π/3, and V_m is the molar volume [14]. The bond valence of ionic atom i (V_i) was defined as the sum of all of the valences from a given atom i:

$$V_i = \sum v_{ij} \quad (5)$$

and v_{ij} is given by

$$v_{ij} = \exp\left(\frac{R_{ij} - d_{ij}}{b'}\right) \quad (6)$$

where R_{ij} is the bond valence parameter, d_{ij} is the length of the bond between atoms i and j, and b' is a universal constant (0.37 Å) [15].

3 Results and discussion

Figure 1(a) presents the XRD patterns of CTLA ceramics (x = 0, 0.3, 0.4, 0.5, 0.6, 0.7, 1) sintered at 1450 ℃ for 4 h. A pure phase of the perovskite structure was obtained in the entire compositional range, and the peaks shifted to higher angles as the $LaAlO_3$ content increased. The phase structure of the CTLA ceramics with $x \leqslant 0.5$ exhibited an orthorhombic perovskite structure similar to that of $CaTiO_3$, while the phase structure of the CTLA ceramics with $x > 0.5$ exhibited a rhombohedral perovskite structure similar to that of $LaAlO_3$. This indicates a phase transition at a composition close to $x = 0.5$. To verify the phase transition, the two strongest peaks, at approximately 33° and 40.8°, are magnified in the composition range of $0.4 \leqslant x \leqslant 0.7$ in Fig. 1(b). The double peaks of the orthorrhombic structure at $x = 0.5$ evolved into the triple peaks of the rhombohedral structure at $x = 0.6$, but the diffraction peaks of the ceramic with $x = 0.5$ were not as sharp as those corresponding to the ceramic with $x = 0.4$. Moon *et al.* [8] reported that the phase transformation orthorhombic (at $x \leqslant 0.4$)→pseudocubic (at $x = 0.5$) → rhombohedral (at $x \geqslant 0.6$) occurs in $(1-x)CaTiO_3$–$xLaAlO_3$ ceramics. Khalyavin *et al.* [10] concluded that increasing the $LaAlO_3$ content in $(1-x)CaTiO_3$–$xLaAlO_3$ microwave ceramics results in two phase transitions: *Pnma* → *Imma* (for $0.4 < x < 0.5$) and *Imma* → $R\bar{3}c$ (for $0.5 < x < 0.6$). Therefore, the diffrence between the diffraction peaks of the ceramics with $x = 0.4$ and $x = 0.5$ could be attributed to a space group transformation.

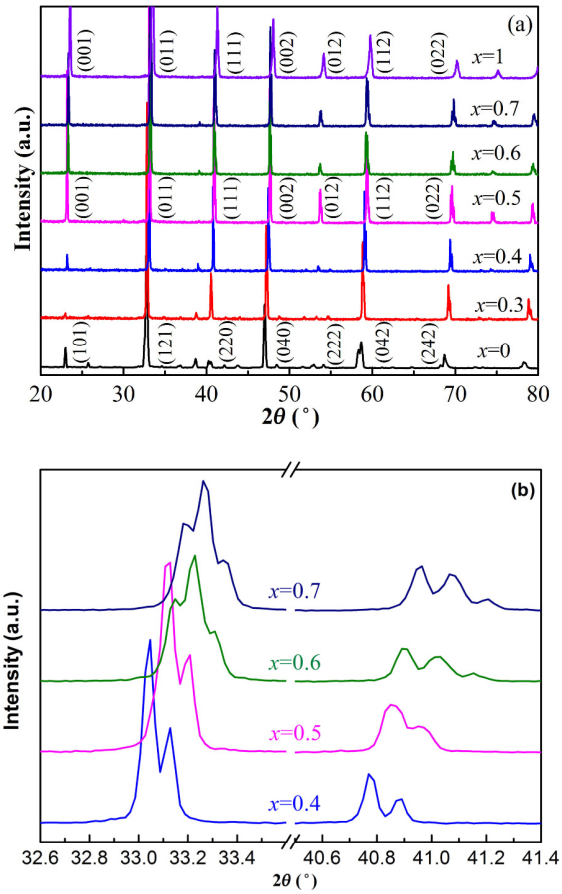

Fig. 1 XRD patterns of the CTLA ceramics sintered at 1450 ℃ for 4 h. (a) XRD patterns of the CTLA ceramics (x = 0, 0.3, 0.4, 0.5, 0.6, 0.7, 1); (b) magnified peaks of the CTLA ceramics (x = 0.4, 0.5, 0.6, 0.7) at 33° and 40.8°.

The lattice parameters of the CTLA ceramics are listed in Table 1. The crystal structure transformed from orthorhombic to rhombohedral as the $LaAlO_3$ content increased. The transformation of the space group was verified to be *Pnma* → *Imma* (for $0.4 < x < 0.5$) and *Imma* → $R\bar{3}c$ (for $0.5 < x < 0.6$), which is consistent

Table 1 Lattice parameters of the CTLA ceramics

x	Structure	Space group	a (Å)	b (Å)	c (Å)	V (Å^3)	Z
0.3	Orthorhombic	*Pnma*	5.4093	7.6458	5.4166	224.02	4
0.4	Orthorhombic	*Pnma*	5.4118	7.6461	5.4125	223.97	4
0.5	Orthorhombic	*Imma*	5.4112	7.6320	5.4034	223.15	4
0.6	Rhombohedral	$R\bar{3}c$	5.4044	—	13.1890	333.61	6
0.7	Rhombohedral	$R\bar{3}c$	5.3966	—	13.1711	332.19	6

with the results of Khalyavin *et al.* [10]. Because the ionic radius of the substitutional Al^{3+} (0.535 Å) is smaller than the ionic radius of Ti^{4+} (0.605 Å), the unit cell volume decreased slightly as the $LaAlO_3$ content increased.

A comparison of the apparent densities and the theoretical densities (calculated from the XRD parameters) is shown in Fig. 2. Both the apparent densities and theoretical densities increased as the $LaAlO_3$ content increased, which can be attributed to the larger molar mass of $LaAlO_3$ compared with $CaTiO_3$. The relative densities (the ratio of the apparent densities to the theoretical densities) were higher than 96% in the entire compositional range; therefore, the influence of density on the microwave dielectric properties could be ignored [16].

SEM images of the CTLA ceramics ($0.3 \leqslant x \leqslant 0.7$) sintered at 1450 ℃ for 4 h are shown in Fig. 3. Figures 3(a)–3(e) are shown at the same magnification and correspond to $x = 0.3$, 0.4, 0.5, 0.6, and 0.7, respectively. Figure 3(f) is presented at a lower magnification to show a larger area of the microstructure of the $x = 0.5$ composition. The grains showed normal growth and were closely packed with few pores. The microstructures revealed that the grains were equiaxed with lamellae grown in all cases except at $x = 0.5$ (shown in Fig. 3(c)). Abnormal grain growth began at $x = 0.5$ and the grain boundaries became irregular and the difference between grain size became exaggerated.

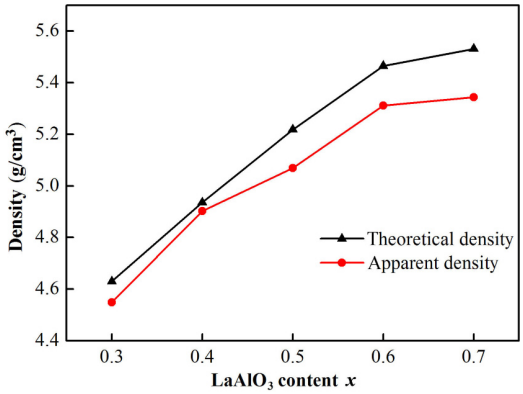

Fig. 2 Densities of the CTLA ceramics sintered at 1450 ℃ for 4 h.

The dielectric constant and the polarizability deviation of the CTLA ceramics sintered at 1450 ℃ for 4 h are shown in Fig. 4. As the content of $LaAlO_3$ increased, both ε_r and polarizability deviation decreased.

The polarizability and the polarizability deviation calculated using Eqs. (2), (3), and (4) are shown in Table 2. The theoretical polarizability increased linearly as the $LaAlO_3$ content increased because the ionic polarizability of $LaAlO_3$ (12.89 $Å^3$) is larger than that of $CaTiO_3$ (12.12 $Å^3$). However, the dielectric constant decreased as the $LaAlO_3$ content increased. The dielectric constant is dependent on the ionic polarizability of the composition, relative density, and secondary phase. The effects of relative density and secondary phase were small, thus the ionic polarizability was the most important factor leading to the decrease of the dielectric constant. Shannon *et al.*

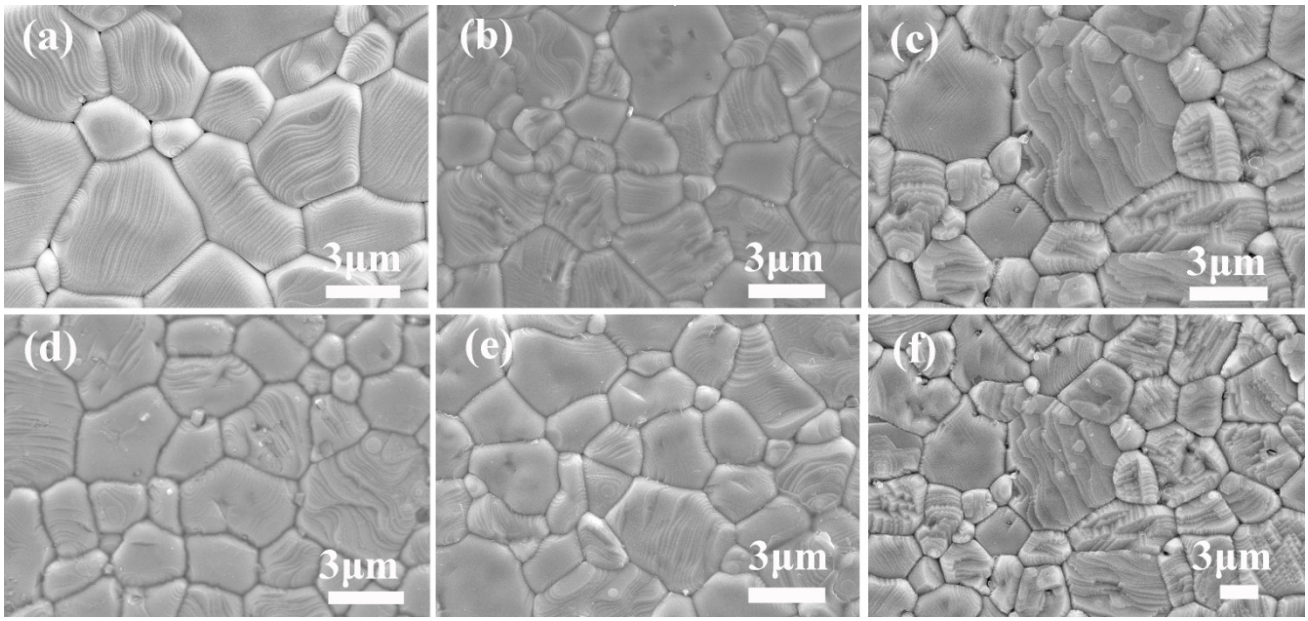

Fig. 3 SEM images of the CTLA ceramics sintered at 1450 ℃ for 4 h: (a) $x = 0.3$, (b) $x = 0.4$, (c) $x = 0.5$, (d) $x = 0.6$, (e) $x = 0.7$, (f) $x = 0.5$.

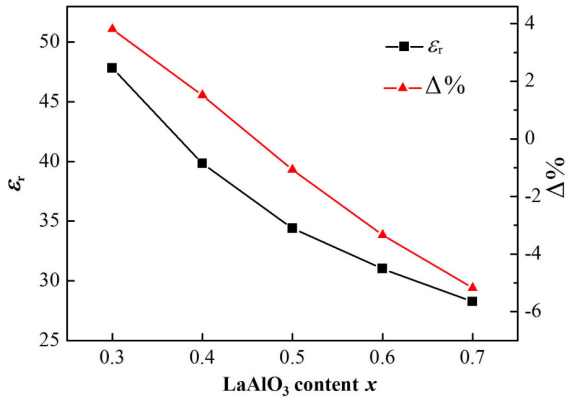

Fig. 4 Dielectric constant (ε_r) and polarizability deviation (Δ%) of the CTLA ceramics sintered at 1450 ℃ for 4 h.

Table 2 Comparison of the observed and theoretical polarizabilities of the CTLA ceramics with different $LaAlO_3$ content sintered at 1450 ℃ for 4 h

x	$\alpha_{theo.}$ (Å^3)	Observed				Δ%
		ε_r	$V_{unit\ cell}$ (Å^3)	Z	$\alpha_{obs.}$ (Å^3)	
0.3	12.351	47.83	224.02	4	12.565	1.74
0.4	12.428	39.83	223.97	4	12.563	1.08
0.5	12.505	34.39	223.15	4	12.363	−1.13
0.6	12.582	31.01	333.61	6	12.180	−3.20
0.7	12.659	28.25	332.19	6	12.016	−5.08

[17] revealed that the cation rattling affects the total polarizability, i.e., it dominates the deviation of polarizability, and subsequently influences the dielectric constant. As x increased from 0.3 to 0.7, the deviation of polarizability decreased from 1.74 to −5.08, which suggests that cation rattling changed with the addition of La^{3+} and Al^{3+}. The positive deviation of polarizability (at $x = 0.3$, 0.4) indicates enhanced cation rattling, while the negative deviation of polarizability (at $x = 0.5$, 0.6, 0.7) indicates reduced cation rattling. Therefore, as x increased, the decreasing deviation of polarizability caused the dielectric constant to decrease. Fu *et al.* [18] reported that the second-order Jahn–Teller distortion decreases as the Ti^{4+} ion content decreases, which can reduce the cation rattling effect and, consequently, reduce the dielectric constant of the ceramics. Fu *et al.*'s conclusion supports the assertion that the dielectric constant is related to the deviation of polarizability, which is used to represent the effect of cation rattling.

The A-site bond valence of the CTLA ceramics sintered at 1450 ℃ for 4 h is shown in Table 3. As x increased, the bond valence of the A-site increased and τ_f decreased. It has been reported that τ_f is closely related to the bond valence of the A-site cation [19,20]. According to bond valence theory, the stronger the bond strength is, the greater the reduction of the rattling effect of the A-site is. A large A-site bond valence indicates that the bond strength between oxygen and the A-site ion is strong, which decreases the rattling effect and, subsequently, decreases τ_f. τ_f decreased significantly at $x = 0.5$, which is attributed to the phase transition from orthorhombic to rhombohedral; similar results were reported by Moon *et al.* [8].

Table 3 A-site bond valance and τ_f of the CTLA ceramics sintered at 1450 ℃ for 4 h

x	$R_{(A-O)}$ (Å)	$d_{(A-O)}$ (Å)	b' (Å)	$v_{(A-O)}$	V_A	τ_f (ppm/℃)
0.3	2.0285	2.7058	0.37	0.1603	1.9240	17.77
0.4	2.0490	2.7056	0.37	0.1696	2.0347	−11.53
0.5	2.0695	2.7023	0.37	0.1808	2.1699	−38.09
0.6	2.0900	2.6993	0.37	0.1927	2.3123	−15.53
0.7	2.1105	2.6954	0.37	0.2058	2.4695	−20.42

The $Q \times f$ values of the CTLA ceramics with different $LaAlO_3$ content sintered at 1450 ℃ are shown in Fig. 5. The $Q \times f$ values increased as the $LaAlO_3$ content increased, except at $x = 0.5$, when it decreased significantly. The $Q \times f$ value of the ceramics depends primarily on intrinsic factors relating to the lattice anharmonicity for a particular composition and crystal structure, and extrinsic factors such as secondary phase, density, and microstructure [21]. In the case of the CTLA ceramics, no secondary phases or impurities were detected, as shown in Figs. 1 and 3, and relative densities were greater than 96%, as shown in Fig. 2. Considering the intrinsic factors, the polarizability deviation and A-site bond valence illustrate that cation rattling was impacted by an external electric field. As x increased, the cation rattling was reduced and $Q \times f$

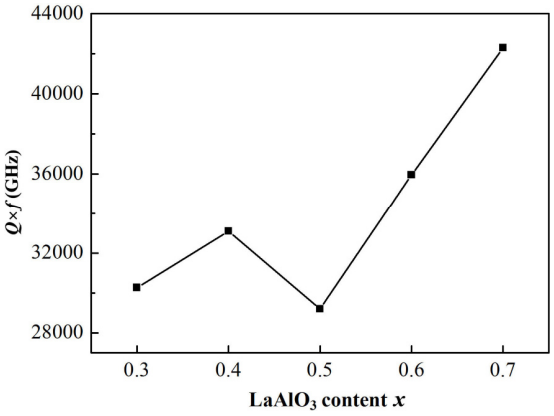

Fig. 5 $Q \times f$ values of the CTLA ceramics sintered at 1450 ℃ for 4 h.

values improved. However, similar to τ_f, the $Q \times f$ value at $x = 0.5$ decreased significantly, which was attributed to the phase transition.

Figure 6 shows the Raman spectra of $(1-x)CaTiO_3$–$xLaAlO_3$ ($x = 0$, 0.3, 0.4, 0.5, 0.6, 0.7, 1) ceramics in the frequency range of 100–1000 cm^{-1}. In $CaTiO_3$ ceramics, the band at 641 cm^{-1} is attributed to Ti–O symmetric stretching vibration and the bands at 469 and 496 cm^{-1} are attributed to Ti–O torsional modes (bending or internal vibration of the oxygen cage). We attribute the bands between 224 and 334 cm^{-1} to the modes associated with rotations of oxygen cage and the band at 180 cm^{-1} to the motion of A-site ions. These conclusions agree with the results reported by Hirata *et al*. [22] and Balachandran and Eror [23]. The major scattering bands were observed in Raman spectrum of $LaAlO_3$. The band below 200 cm^{-1} can be attributed to the mode related to the motion of La^{3+} ions, and the band at 483 cm^{-1} results from the internal vibration of the oxygen cage. As the value of x increased from 0.3 to 0.7, several peaks were split and new Raman-active modes appeared. In the CTLA ceramics, Ti^{4+} and Al^{3+} are distributed uniformly throughout the B-sites. The broad mode around 800 cm^{-1} (A_{1g}) which indicates the short-range order of B-site cation was absent in the spectra from both pure $LaAlO_3$ and $CaTiO_3$ but present in the spectra of CTLA ($0.3 \leqslant x \leqslant 0.7$) ceramics. This mode is typically observed in complex perovskite solid solutions [24]. The higher the Raman peak is and the narrower the full-width at half-maximum of the peak is, the higher the degree of short-range order is, which contributes to lower dielectric loss and results in higher $Q \times f$ values. Compared with the other Raman peaks in the band A_{1g}, the peak for the $x = 0.5$ composition was the lowest and the broadest, which suggests that the short-range order degree of B-sites was at a minimum. This agrees with our other results and explains why the $x = 0.5$ composition has the lowest $Q \times f$.

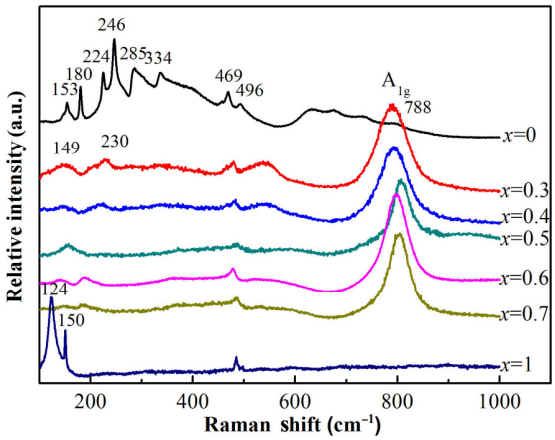

Fig. 6 Raman spectra from $(1-x)CaTiO_3$–$xLaAlO_3$ solid solutions.

4 Conclusions

We prepared $(1-x)CaTiO_3$–$xLaAlO_3$ ($0 \leqslant x \leqslant 1$) microwave dielectric ceramics using a conventional two-step solid-state reaction method. The effects of structural transformation and ionic-parameters such as polarizability, cation rattling, A-site bond valence, and the order degree of the B-site cation on microwave dielectric properties were studied. The dielectric constant decreased from 47.83 to 28.25 as the $LaAlO_3$ content in the CTLA ceramics increased from 0.3 to 0.7 because the polarizability deviation decreased from 1.74 to −5.08. As the $LaAlO_3$ content increased, the temperature coefficient of the resonant frequency decreased from 17.77 to −20.42 ppm/℃ because the A-site valence increased from 1.9240 to 2.4695, and $Q \times f$ value increased from 30 000 to 42 000 GHz because the cation rattling reduced and the order degree of B-site ions increased. A structural transformation occurred at $x = 0.5$, which deteriorated the temperature coefficient of the resonant frequency and $Q \times f$ value.

References

[1] Jiang J, Fang D, Lu C, *et al*. Solid-state reaction mechanism and microwave dielectric properties of $CaTiO_3$–$LaAlO_3$ ceramics. *J Alloys Compd* 2015, **638**: 443–447.

[2] Vidmar M, Golobič A, Meden A, *et al*. Sub-solidus phase relations and a structure determination of new phases in the CaO–La_2O_3–TiO_2 system. *J Eur Ceram Soc* 2015, **35**: 2801–2814.

[3] Zhang X, Zhang Y, Zhang J, *et al*. Microwave dielectric properties and thermally stimulated depolarization currents study of $(1-x)Ba_{0.6}Sr_{0.4}La_4Ti_4O_{15}$–$xTiO_2$ ceramics. *J Am Ceram Soc* 2014, **97**: 3170–3176.

[4] Sebastian MT. *Dielectric Materials for Wireless Communication*. Elsevier Science Publishers, 2008: 165, 172.

[5] Cho S-Y, Kim I-T, Hong KS. Microwave dielectric properties and applications of rare-earth aluminates. *J Mater Res* 1999, **14**: 114–119.

[6] Grebenshchikov RG, Popova VF, Shirvinskaya AK. Phase diagrams of the $LnAlO_3$–$CaTiO_3$ (Ln = Nd, Sm) systems and polymorphism of $CaTiO_3$. *Glass Phys Chem*+ 2003, **29**: 194–199.

[7] Grebenshchikov RG, Popova VF, Shirvinskaya AK. Solid solutions in the $LnAlO_3$–$CaTiO_3$ (*Ln* = Dy, Y, Lu) systems.

Glass Phys Chem+ 2003, **29**: 479–483.
[8] Moon JH, Jang HM, Park HS, *et al*. Sintering behavior and microwave dielectric properties of (Ca, La)(Ti, Al)O_3 ceramics. *Jpn J Appl Phys* 1999, **38**: 6821–6826.
[9] Hou G, Wang Z, Zhang F. Sintering behavior and microwave dielectric properties of $(1-x)CaTiO_3$–$xLaAlO_3$ ceramics. *J Rare Earth* 2011, **29**: 160–163.
[10] Khalyavin DD, Salak AN, Senos AMR, *et al*. Structure sequence in the $CaTiO_3$–$LaAlO_3$ microwave ceramics—Revised. *J Am Ceram Soc* 2006, **89**: 1721–1723.
[11] Zhang C, Zuo R, Zhang J, *et al*. Structure-dependent microwave dielectric properties and middle-temperature sintering of forsterite $(Mg_{1-x}Ni_x)_2SiO_4$ ceramics. *J Am Ceram Soc* 2015, **98**: 702–710.
[12] Huang C-L, Yang W-R, Yu P-C. High-Q microwave dielectrics in low-temperature sintered $(Zn_{1-x}Ni_x)_3Nb_2O_8$ ceramics. *J Eur Ceram Soc* 2014, **34**: 277–284.
[13] Li J, Han Y, Qiu T, *et al.* Effect of bond valence on microwave dielectric properties of $(1-x)CaTiO_3$–$x(Li_{0.5}La_{0.5})TiO_3$ ceramics. *Mater Res Bull* 2012, **47**: 2375–2379.
[14] Shannon RD. Dielectric polarizabilities of ions in oxides and fluorides. *J Appl Phys* 1993, **73**: 348–366.
[15] Brese NE, O'Keeffe M. Bond-valence parameters for solids. *Acta Cryst* 1991, **B47**: 192–197.
[16] Zhang P, Zhao Y, Wang X. The correlations between electronic polarizability, packing fraction, bond energy and microwave dielectric properties of $Nd(Nb_{1-x}Sb_x)O_4$ ceramics. *J Alloys Compd* 2015, **644**: 621–625.
[17] Shannon RD, Dickinson JE, Rossman GR. Dielectric constants of crystalline and amorphous spodumene, anorthite and diopside and the oxide additivity rule. *Phys Chem Miner* 1992, **19**: 148–156.
[18] Fu MS, Ni L, Chen XM. Abnormal variation of microwave dielectric properties in A/B site co-substituted $(Ca_{1-0.3x}La_{0.2x})[(Mg_{1/3}Ta_{2/3})_{1-x}Ti_x]O_3$ complex perovskite ceramics. *J Eur Ceram Soc* 2013, **33**: 813–823.
[19] Cho YS, Yoon KH, Lee BD, *et al*. Understanding microwave dielectric properties of Pb-based complex perovskite ceramics via bond valence. *Ceram Int* 2004, **30**: 2247–2250.
[20] Kim ES, Chun BS, Freer R, *et al*. Effects of packing fraction and bond valence on microwave dielectric properties of $A^{2+}B^{6+}O_4$ (A^{2+}: Ca, Pb, Ba; B^{6+}: Mo, W) ceramics. *J Eur Ceram Soc* 2010, **30**: 1731–1736.
[21] Li L, Cai H, Yu X, *et al*. Structure analysis and microwave dielectric properties of $Ca_xZn_{1-x}Sn_{0.08}Ti_{1.92}Nb_2O_{10}$ ceramics. *J Alloys Compd* 2014, **584**: 315–321.
[22] Hirata T, Ishioka K, Kitajima M. Vibrational spectroscopy and X-ray diffraction of perovskite compounds $Sr_{1-x}M_xTiO_3$ (M = Ca, Mg; $0 \leqslant x \leqslant 1$). *J Solid State Chem* 1996, **124**: 353–359.
[23] Balachandran U, Eror NG. Laser-induced Raman scattering in calcium titanate. *Solid State Commun* 1982, **44**: 815–818.
[24] Zheng H, Csete de Györgyfalva GDC, Quimby R, *et al*. Raman spectroscopy of B-site order–disorder in $CaTiO_3$-based microwave ceramics. *J Eur Ceram Soc* 2003, **23**: 2653–2659.